

Wilson–Fisher Renormalization of Discrete Gravity–Capillary Wave Turbulence in Viscous Fluids

José A. Santiago,^{1,2} Mikheil Kharbedia,^{1,3} Basilio J. García,⁴ and Francisco Monroy^{1,3,*}

¹Departamento de Química Física, Universidad Complutense de Madrid, 28040 Madrid, Spain

²Departamento de Matemáticas Aplicadas y Sistemas Universidad Autónoma

Metropolitana Cuajimalpa Vasco de Quiroga 4871, 05348 Cd. de México, Mexico.

³Translational Biophysics, Instituto de Investigación Sanitaria Hospital 12 de Octubre, 28041 Madrid, Spain[†]

⁴Departamento de Física Aplicada, Universidad Autónoma de Madrid, 28049 Madrid, Spain

(Dated: January 16, 2026)

We report an experimental realization of Wilson–Fisher renormalization in driven surface-wave turbulence across Newtonian fluids spanning nearly six decades in Reynolds number. Discrete capillary and gravity turbulence define two universality classes selected by interaction topology: triadic resonances for capillary waves and effectively tetradiac scattering for gravity waves. Navier–Stokes viscosity is the relevant perturbation that renormalizes spectral transfer and terminates the cascade. The resulting framework predicts the Kolmogorov cutoff from the balance of nonlinear transfer and viscous damping, and Reynolds scaling of the integrated inertial spectral weight. Laser Doppler vibrometry quantitatively confirms these renormalized scaling laws, establishing discrete gravity–capillary turbulence as a tunable laboratory for nonequilibrium crossover criticality.

Universality in turbulence reflects the separation between inertial transfer and dissipation [1]. In fully developed hydrodynamic turbulence, Kolmogorov’s phenomenology identifies an inertial cascade terminated at small scales by viscous dissipation [2, 3]. This scale separation can be phrased in Wilsonian terms [4]: coarse graining integrates out fast degrees of freedom to yield scale-dependent effective dynamics, while relevant perturbations—viscosity as the paradigmatic example, control departures from scale invariance [5]. A long-standing renormalization-group (RG) program for Navier–Stokes (NS) turbulence follows this logic [6–8], using RG flows to predict renormalized transport [9] and functional scaling [10, 11]. By contrast, wave turbulence (WT) theory is largely formulated around inviscid fixed points [12, 13] and, despite renormalization procedures for interactions and spectra [8, 11], lacks a Wilsonian organization of viscous crossover flows in experimentally accessible RG coordinates. Here we adopt a Wilson–Fisher (WF) viewpoint, where relevant perturbations control the approach to scale-invariant fixed points and generate observable crossover scaling [14].

Nonlinear surface waves, including gravity (GW) and capillary (CW) modes, provide a canonical setting where dispersion selects the resonant interaction channels [15]. In the weak regime, they support Kolmogorov–Zakharov (KZ) fixed points with surface-velocity spectra $S(\omega) \sim \omega^{-p}$ [12, 13]. As summarized in Fig. 1, CW and GW turbulence define two universality classes set by interaction topology: CW is governed by exact three-wave resonances, whereas deep-water GW forbids triads and is controlled by effective four-wave (tetradiac) scattering via quasi-resonant quartets [15]. In both classes, spectral discreteness persists across the inertial range, while viscosity terminates the cascade at the Kolmogorov cutoff ω_K —dispersion selects the class, dissipation sets exit.

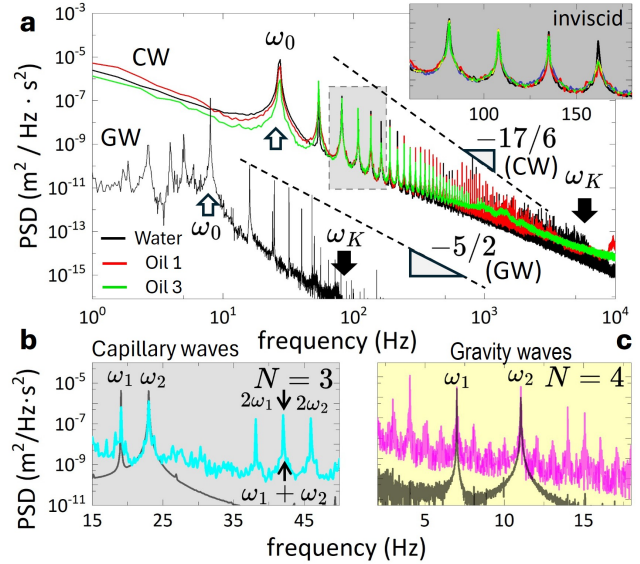


FIG. 1. Frequency-domain signatures and inertial scaling of discrete surface-wave turbulence (DSWT) in viscous fluids. (a) Broadband surface-velocity power spectral density $S(\omega)$ showing the capillary-wave (CW; top) and gravity-wave (GW; bottom) cascades for water and high-viscosity oils (Oil 1: 10, Oil 3: 10^3 times the viscosity of water). Open arrows mark the excitation frequency ω_0 , filled ones the Kolmogorov cutoff ω_K . Dashed guide lines indicate KZ scaling: $S(\omega) \sim \omega^{-17/6}$ (CW) and $S(\omega) \sim \omega^{-5/2}$ (GW). Inset: discrete inviscid CW modes persist across the inertial range, essentially independent of bulk viscosity. (b) CW spectrum illustrating three-wave ($N = 3$) resonant mixing, with peaks at $\omega_1, \omega_2, 2\omega_1, 2\omega_2$, and $\omega_1 + \omega_2$. (c) GW spectrum illustrating four-wave ($N = 4$) transfer, with dominant peaks at ω_1, ω_2 and dismutation resonances.

In this Letter, we develop and test a Wilsonian framework for discrete surface-wave turbulence (DSWT) under monochromatic forcing at ω_0 , where dissipation controls the crossover dynamics of the GW and CW cas-

cade response (Fig. 1). We cast this behavior in a Wilson–Fisher (WF) picture [4, 14]: interaction topology selects conservative fixed points, while Navier–Stokes viscosity is the relevant perturbation that renormalizes transfer and terminates the inertial interval at a viscous (Kolmogorov) cutoff ω_K (Fig. 1a). Using laser Doppler vibrometry (LDV) [16, 17], we first observe a robust capillary-wave inertial cascade with the expected KZ decay of the surface-velocity PSD, $S(\omega) \sim \omega^{-17/6}$ for $\omega > \omega_0$ [13], persisting without measurable resonance broadening over nearly three decades of viscosity (Fig. 1a; inset). This invariance is consistent with exact three-wave resonances in dispersive CWs, $\mathbf{k}_1 + \mathbf{k}_2 = \mathbf{k}_3$ and $\omega_1 + \omega_2 = \omega_3$ (i.e., detuning $\Delta \equiv \omega_1 + \omega_2 - \omega_3 = 0$), indicating strictly conservative triadic coupling (Fig. 1b), as described in Kartashova’s theory of discrete wave turbulence [18, 19]. By contrast, in the GW branch we observe a direct inertial decay consistent with the weak-turbulence prediction $S(\omega) \sim \omega^{-5/2}$ for $\omega > \omega_0$ [20]. An enhanced subharmonic response appears below ω_0 (Fig. 1a, bottom), consistent with weak reverse transfer and *dismutation* signatures [19, 20]. In dismutation, two pumped modes (ω_1, ω_2) scatter into a frequency-split quartet, generating one daughter above the pumped band and one below (Fig. 1c). Intraband products may also arise via harmonics/subharmonics of pumping. This is consistent with quasi-elastic tetradic scattering, $\mathbf{k}_1 + \mathbf{k}_2 = \mathbf{k}_3 + \mathbf{k}_4$, where the frequency condition is quasi-resonant, $\omega_1 + \omega_2 = \omega_3 + \omega_4 + \Delta$ with small detuning $\Delta \neq 0$, reflecting resonance broadening for underdispersive gravity waves $\omega_G \propto k^{1/2}$ [13, 20] and inexact resonance clustering [18, 19].

Our analysis exploits a systematic dataset acquired across Newtonian fluids with variable surface tension σ and density ρ , spanning more than three decades in dynamic viscosity η , including water and silicone oils (Table I). The surface-velocity spectrum is driven monochromatically at angular frequency ω_0 with displacement amplitude A , measured noninvasively by laser Doppler vibrometry (LDV) [16, 17]. Across fluids, the kinematic viscosity $\nu = \eta/\rho$ spans $\sim 10^4$ and, over the explored ω_0 range, the LDV-resolved forcing velocity $U_0 \equiv A\omega_0$ spans $\sim 10^3$, enabling a wide sweep of Reynolds number, $\text{Re} \equiv U_0\Lambda_0/\nu$, while keeping the injection scale Λ_0 comparable. The drive selects the forcing wavenumber k_0 via the linear dispersion relation (GW/CW); we define the injection length $\Lambda_0 \equiv 2\pi/k_0$, and the injected kinetic-energy density $E = \frac{1}{2}\rho U_0^2$. In all fluids, both CW and GW branches display direct KZ-type cascades for $\omega > \omega_0$, extending over a discrete inertial interval that terminates at the viscous cutoff ω_K (Fig. 1a). These experimentally resolved features motivate a WF organization in terms of two reduced RG coordinates: the ultraviolet-to-injection viscous-rate ratio $\bar{\Omega} \equiv \omega_K/(\nu k_0^2)$ and the integrated inertial spectral weight $\Sigma_{\text{PSD}} = \int_{\omega_0}^{\omega_K} S(\omega) d\omega$, which quantifies the global

TABLE I. Material parameters of the fluids used in the DSWT experiments, ordered by increasing kinematic viscosity ν . Surface tension σ , density ρ , and dynamic viscosity η are shown to emphasize that kinematic viscosity acts as the primary relevant perturbation in the RG flow.

Fluid	σ (mN m $^{-1}$)	η (mPas)	ρ (g cm $^{-3}$)	ν (mm 2 s $^{-1}$)
Mercury	487	1.6	13.6	0.12
n-Hexane	18	0.30	0.70	0.43
Chloroform	27	0.54	1.50	0.47
CCl ₄	27	1.0	1.60	0.63
Water (Milli-Q)	72	0.82	1.00	0.82
Pb(NO ₃) ₂ (sat.)	90	2.5	1.30	2.3
Oil 1 (RTM8)	32	10	0.80	13
Oil 2 (RTM14)	32	100	0.80	125
Glycerol	63	1410	1.30	1100
Oil 3 (RTM18)	32	1000	0.80	1250

cascade response to forcing. In addition, GW spectra exhibit subharmonic dismutation signatures (Fig. 1c) and enhanced response below ω_0 (Fig. 1a, bottom), consistent with weak reverse transfer and a much smaller spectral weight than CW, $\Sigma_{\text{PSD}}^{(G)} \approx 10^{-3}\Sigma_{\text{PSD}}^{(C)}$, yielding two energetically well separated, non-overlapping responses. This WF structure predicts the scaling of $\bar{\Omega}$ with E and the Reynolds renormalization of the reduced cascade response $\bar{\Sigma} \equiv \Sigma_{\text{PSD}}/(\Lambda_0\omega_0)^2$, yielding distinct RG exponents for triadic capillary and tetradic gravity cascades. Unlike WT treatments focused on fixed-point spectra, promoting $\bar{\Omega}$ and $\bar{\Sigma}$ to RG coordinates enables direct observation of crossover trajectories and organizes DSWT into two topology-defined attraction basins.

Wilson–Fisher renormalization framework.— In the inviscid limit, surface-wave turbulence is governed by resonant interactions constrained by dispersion, leading to scale-invariant KZ–spectra in the inertial interval [12, 13]. In Wilson–Fisher (WF) language, these KZ states act as conservative fixed points, while the interaction topology—triadic for capillary waves and effectively tetradic for gravity waves (Fig. 1), selects the universality class [20, 21]. To render the RG structure explicit, we introduce a running frequency scale ω and define as dimensionless coupling the squared wave steepness

$$g(\omega) \equiv \epsilon(\omega)^2 \sim k(\omega)^2 S(\omega) \omega, \quad (1)$$

where $S(\omega)$ is the surface-velocity spectrum and $k(\omega)$ follows from the linear dispersion relation [15]. Writing $S(\omega) \sim \omega^{-p}$, one has $g(\omega) \sim \omega^{y_g}$ with

$$y_g \equiv 2\alpha - (p - 1), \quad k(\omega) \sim \omega^\alpha, \quad (2)$$

and the RG “time” $\ell \equiv \ln(\omega/\omega_0)$. The coarse-graining flow is then captured at scaling level by a WF beta function [4, 22] (see SM for details),

$$\beta(g) \equiv \frac{dg}{d\ell} = y_g g - B_N g^{N-1}, \quad (3)$$

where $B_N > 0$ encodes nonlinear saturation and the interaction topology enters through the order N of the resonant process. (End Matter connects the topology of the interaction vertex to the saturation term.) Besides the Gaussian fixed point $g^* = 0$, Eq. (3) admits a nontrivial stable fixed point $g^* \sim (y_g/B_N)^{1/(N-2)}$ corresponding to the KZ inertial state. In the weak regime we use $p = 17/6$ (capillary) and $p = 5/2$ (gravity) [12, 13].

Kolmogorov scale. NS-viscosity explicitly breaks the inviscid scale invariance and provides the RG-relevant perturbation that drives the system away from each conservative fixed point [6]. For small-amplitude surface waves, linear viscous hydrodynamics yields a damping rate $\gamma_\nu(k) \propto \nu k^2$ and a viscous time $\tau_\nu(k) \approx (\nu k^2)^{-1}$ [1, 23]. This Kolmogorov UV-relevant dissipative operator is common to both CW/GW turbulence because it is inherited directly from the bulk NS-term $\nu \nabla^2 \mathbf{u}$ [1]; the only regime dependence enters through the nonlinear transfer time, which is set by the interaction topology.

Fixed points: universality classes. The inertial interval terminates at the experimentally resolved Kolmogorov cutoff ω_K (Fig. 1a), selected by the crossover condition $\tau_{\text{nl}}(\omega_K) \approx \tau_\nu(\omega_K)$, in direct analogy with Kolmogorov's dissipation scale [2, 3, 13]. To make explicit how interaction topology enters this cutoff, we relate the nonlinear rate to the inertial spectrum at scaling level. For a narrow band around ω , the typical wave amplitude satisfies $a_\omega^2 \sim S(\omega) \omega$, while the dimensionless nonlinearity is the steepness $\epsilon(\omega) \sim k(\omega) a_\omega$. In weak turbulence, the kinetic transfer rate generated by an N -wave resonant process scales as $\tau_{\text{nl}}^{-1}(\omega) \sim \omega \epsilon(\omega)^{2(N-2)}$ [12], so that

$$\tau_{\text{nl}}^{-1}(\omega) \sim \omega [k(\omega)^2 S(\omega) \omega]^{N-2}, \quad N = \begin{cases} 3 & (\text{CW triads}) \\ 4 & (\text{GW tetrads}) \end{cases} \quad (4)$$

(details and prefactors are given in the SM). Because $\tau_\nu^{-1} \approx \nu k^2$ is inherited universally from Navier–Stokes, while τ_{nl} depends on the interaction order N and the KZ exponent p , the ultraviolet cutoff scaling is class-dependent even though the viscous substrate is universal.

We take the injected kinetic-energy density at the driven mode as $E = \frac{1}{2} \rho U_0^2$ with $U_0 \equiv A \omega_0$, and interpret the measured ω_K as the ultraviolet RG scale at which the flow exits the inertial basin. Furthermore, we define a Reynolds-like reduced injected energy $\bar{E} \equiv E \Lambda_0^2 / (\rho \nu^2) = \frac{1}{2} (U_0 \Lambda_0 / \nu)^2 = \frac{1}{2} \text{Re}^2$, which provides a dimensionless forcing coordinate at the injection scale. The WF crossover framework then yields the experimentally testable cutoff laws for each universality class

$$\bar{\Omega}_\nu^{(\text{CW})} \sim \bar{E}^{2/3} \quad (N = 3), \quad \bar{\Omega}_\nu^{(\text{GW})} \sim \bar{E}^1 \quad (N = 4). \quad (5)$$

Cascade energy: Reynolds renormalization.— Beyond the ultraviolet coordinate $\bar{\Omega}_\nu \equiv \omega_K / (\nu k_0^2)$, a second RG observable is the integrated inertial spectral weight $\Sigma_{\text{PSD}} = \int_{\omega_0}^{\omega_K} S(\omega) d\omega$, which measures the total velocity variance accumulated in the direct cascade

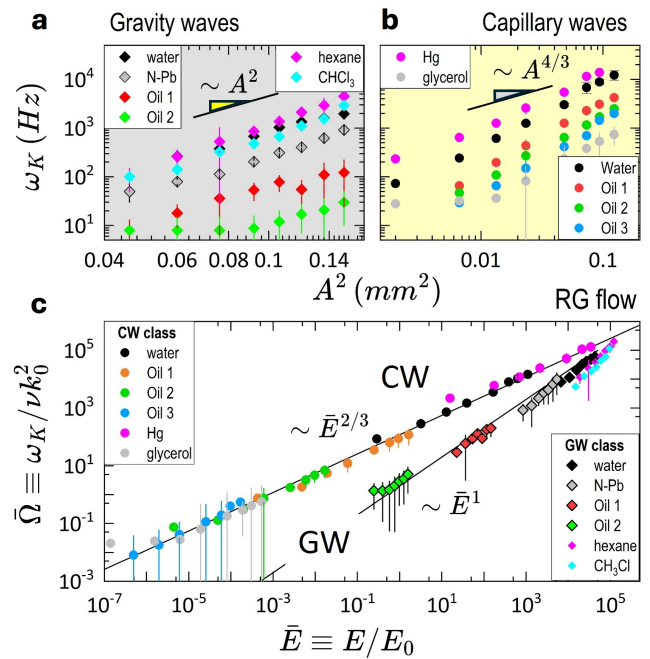


FIG. 2. Kolmogorov cutoff as a Wilson–Fisher ultraviolet scale. (a) GW ($\omega_0 = 8$ Hz): ω_K vs forcing amplitude A . (b) CW ($\omega_0 = 27$ Hz): ω_K vs A . In both regimes, ω_K grows monotonically with forcing, defining the Kolmogorov exit scale. (c) Wegner scaling of the ultraviolet coordinate $\bar{\Omega}_\nu \equiv \omega_K / (\nu k_0^2)$ with $k_0 = 2\pi/\Lambda_0$ and Λ_0 the dispersion-selected forcing length, versus reduced injected energy $\bar{E} \equiv E/E_0$, with $E = \rho(A\omega_0)^2/2$ and $E_0 = \rho(\nu/\Lambda_0)^2$ the viscous kinetic-energy scale at Λ_0 (see SM). Data collapse onto topology-selected branches: $\bar{\Omega}_\nu \sim \bar{E}^1$ (GW, $N = 4$) and $\bar{\Omega}_\nu \sim \bar{E}^{2/3}$ (CW, $N = 3$). Solid lines: Wilson–Fisher predictions from Eq. (5).

between the pump and the UV-exit scale ω_K . The corresponding raw response $\Sigma_{\text{PSD}}(U_0)$ is shown in Supplementary Fig. S1: it increases monotonically with forcing velocity $U_0 = A\omega_0$ in both universality classes, yet remains separated by ~ 3 decades, reflecting a much weaker GW cascade. To expose universal renormalization under injection, we define the reduced response $\bar{\Sigma}_\omega(\text{Re}) \equiv \Sigma_{\text{PSD}} / (\Lambda_0 \omega_0)^2$ with $\Lambda_0 = 2\pi/k_0$ and $\text{Re} \equiv U_0 \Lambda_0 / \nu$. Within the WF crossover framework, $\bar{\Sigma}$ obeys a Wegner scaling form $\bar{\Sigma}(\text{Re}) \sim \text{Re}^{\kappa_N} \mathcal{F}_N(\text{Re}/\text{Re}_\times)$ [22]; in the asymptotic regime, the renormalization exponent is fixed by interaction topology and by the fact that $\bar{\Sigma}_\omega$ probes a quadratic (second-moment) cascade response (see SM), giving $\kappa_N = 2/(N-1)$ and thus

$$\bar{\Sigma}_\omega^{(\text{CW})} \sim \text{Re}^1 \quad (N = 3), \quad \bar{\Sigma}_\omega^{(\text{GW})} \sim \text{Re}^{2/3} \quad (N = 4), \quad (6)$$

quantitatively confirmed by the collapse in Fig. 3.

Discussion.— The central outcome is a genuinely Wilsonian organization of discrete surface-wave turbulence (DSWT): the experimentally accessible coordinates $(\bar{\Omega}_\nu, \bar{\Sigma}_\omega)$ provide a two-parameter RG chart in which monochromatically forced DSWT separates into two at-

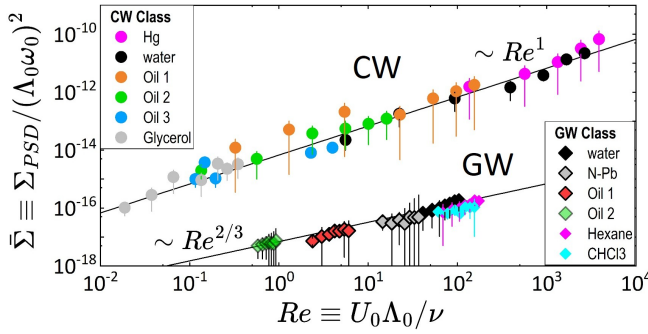


FIG. 3. Reynolds-number renormalization of the cascade response. Reduced inertial spectral weight $\bar{\Sigma} \equiv \Sigma_{\text{PSD}}/(\Lambda_0 \omega_0)^2$ versus $Re \equiv U_0 \Lambda_0 / \nu$ across all fluids, revealing two energetically separated universality classes: capillary-wave (CW, upper) and gravity-wave (GW, lower) turbulence. Data follow WF/Wegner scaling and collapse onto topology-controlled power laws $\bar{\Sigma}_\omega \sim Re^{2/(N-1)}$: $\bar{\Sigma} \sim Re^1$ for CW ($N = 3$) and $\bar{\Sigma}_\omega \sim Re^{2/3}$ for GW ($N = 4$) (solid lines: WF predictions from Eq. (6)), demonstrating interaction-topology renormalization of the global cascade response (SM; End Matter).

traction basins, each governed by a distinct conservative KZ fixed point selected by interaction topology ($N = 3$ for CW and $N = 4$ for GW). *Conceptual punchline*: DSWT admits a Wilsonian RG constructed from directly measured exit and response coordinates, which organize the dynamics into topology-defined basins of attraction. NS-viscosity plays the role of a single relevant perturbation that generates crossover trajectories and terminates the inertial flow at the exit scale ω_K . The simultaneous verification of the Wegner-like law $\bar{\Omega}_\nu(\bar{E})$ (Fig. 2) and the Reynolds renormalization $\bar{\Sigma}_\omega(Re)$ (Fig. 3) thus constitutes a direct experimental realization of WF-crossover criticality in a nonequilibrium cascade (End Matter, Fig. 4 gives a diagrammatic representation of the triadic and tetradiac interaction channels). Beyond providing a controlled laboratory for RG ideas long pursued in NS turbulence, DSWT offers a tunable setting where the universality class is switched by dispersion, while the relevant perturbation is continuously dialed by viscosity. Finally, the two RG coordinates probe complementary pieces of the WF structure: the ultraviolet exit coordinate $\bar{\Omega}_\nu(N, y_g)$ is fixed by the relevance of the steepness coupling under ω -coarse graining, set by topology N and the engineering exponent y_g in $\beta(g) = y_g g - B_N g^{N-1}$, whereas the integrated quadratic response $\bar{\Sigma}_\omega(N, B_N; g_0^2)$ is set by nonlinear saturation, hence by the same topology through B_N and the combinatorial power $N - 1$.

Conclusion.— Discrete gravity and capillary wave turbulence realize two Wilson–Fisher universality classes with topology-selected fixed points and viscosity-controlled crossover. The resulting RG coordinates $(\bar{\Omega}, \bar{\Sigma})$ are directly measurable and obey distinct renormalized scaling laws, establishing DSWT as a tunable platform for nonequilibrium Wilsonian criticality.

We thank Prof. M. G. Velarde for insightful discussions on the role of dimensionless numbers in turbulence. This work was supported by the Agencia Estatal de Investigación (AEI, Spain) under Grants TED2021-132296B-C52 and CPP2024-011880, and by Fundación BBVA–Fundamentos 2025 (to F.M.), and by the Secretaría de Ciencia, Humanidades, Tecnología e Innovación (SECI-HTI, Mexico) under Grant CBF-2025-I-4418 (to J.A.S.).

* monroy@ucm.es

† Present address: Advanced Research Center for Nanolithography (ARCNL), Science Park 106, 1098 XG Amsterdam, The Netherlands

- [1] L. D. Landau and E. M. Lifshitz, *Fluid Mechanics*, 2nd ed., Course of Theoretical Physics, Vol. 6 (Pergamon Press, 1987).
- [2] A. N. Kolmogorov, *Dokl. Akad. Nauk SSSR* **30**, 301 (1941).
- [3] U. Frisch, *Turbulence: The Legacy of A. N. Kolmogorov* (Cambridge University Press, 1995).
- [4] K. G. Wilson and J. Kogut, *Physics Reports* **12**, 75 (1974).
- [5] M. E. Fisher, *Reviews of Modern Physics* **46**, 597 (1974).
- [6] H. W. Wyld, *Annals of Physics* **14**, 143 (1961).
- [7] D. Forster, D. R. Nelson, and M. J. Stephen, *Physical Review A* **16**, 732 (1977).
- [8] G. L. Eyink and N. Goldenfeld, *Physical Review E* **50**, 4679 (1994).
- [9] V. Yakhot and S. A. Orszag, *Journal of Scientific Computing* **1**, 3 (1986).
- [10] L. M. Smith and S. L. Woodruff, *Annual Review of Fluid Mechanics* **30**, 275 (1998).
- [11] L. Canet, *Journal of Fluid Mechanics* **950**, P1 (2022).
- [12] V. E. Zakharov, V. S. L'vov, and G. Falkovich, *Kolmogorov Spectra of Turbulence I: Wave Turbulence* (Springer, 1992).
- [13] S. Nazarenko, *Wave Turbulence* (Springer, 2011).
- [14] K. G. Wilson and M. E. Fisher, *Physical Review Letters* **28**, 240 (1972).
- [15] F. Dias and C. Kharif, *Annual Review of Fluid Mechanics* **31**, 301 (1999).
- [16] P. Cobelli, A. Prasadka, P. Petitjeans, G. Lagubeau, and V. Pagneux, *Physical Review Letters* **103**, 204301 (2009).
- [17] M. Kharbedia, H. López-Menéndez, B. J. García, M. G. Velarde, and F. Monroy, *Advanced Science* **12**, 2407528 (2025).
- [18] E. Kartashova, *Physical Review Letters* **98**, 214502 (2007).
- [19] E. Kartashova, *Europhysics Letters* **87**, 44001 (2009).
- [20] A. I. Dyachenko, A. C. Newell, A. Pushkarev, and V. E. Zakharov, *Physical Review Letters* **92**, 134501 (2004).
- [21] V. E. Zakharov and N. N. Filonenko, *Journal of Applied Mechanics and Technical Physics* **8**, 37 (1967).
- [22] F. J. Wegner, *Phys. Rev. B* **5**, 4529 (1972).
- [23] H. Lamb, *Hydrodynamics*, 6th ed. (Cambridge University Press, 1932).

END MATTER: DIAGRAMMATIC ORIGIN OF TOPOLOGY-DEPENDENT RG FLOWS

Weak wave turbulence can be described as resonant coupling between wave modes, encoded by effective interaction vertices [13, 18, 21]. Figure 4 summarizes the minimal diagrammatic content needed here: the lowest-order resonant process fixes the interaction topology and thus the universality class. Capillary waves (CW) admit exact three-wave resonances (triads, $N = 3$). Deep-water gravity waves (GW) forbid exact triads, so transfer proceeds through effective four-wave interactions (tetrads, $N = 4$), with a finite resonance width (schematically indicated by a detuning insertion $\Delta \neq 0$). Under Wilsonian coarse graining, this topology controls the leading nonlinear saturation of the running coupling $g(\omega) = \epsilon(\omega)^2$ and yields a Wilson–Fisher beta function $\beta(g) = y_g g - B_N g^{N-1}$, where the power $N - 1$ is fixed by the dominant vertex.

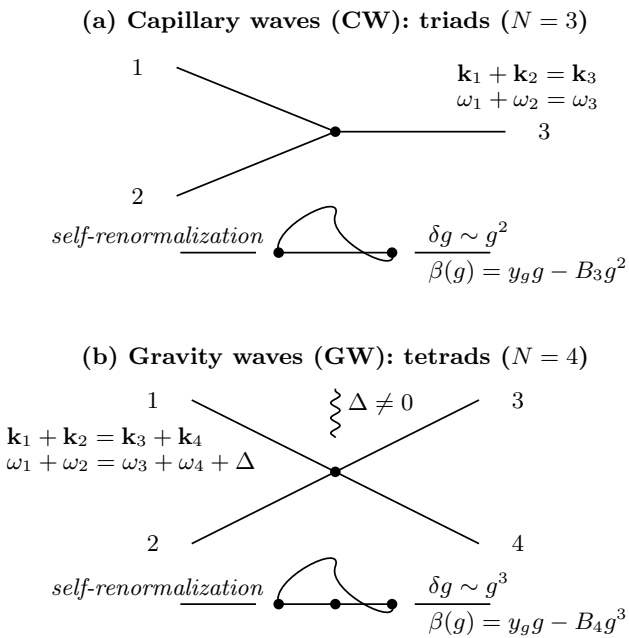


FIG. 4. **Topology-dependent interaction vertices and WF saturation at fixed points.** (a) Capillary-wave turbulence admits exact triads ($N = 3$), yielding $\delta g \sim g^2$ and $\beta(g) = y_g g - B_3 g^2$. (b) Deep-water gravity-wave turbulence proceeds via effective tetrads ($N = 4$) with finite resonance broadening (detuning insertion $\Delta \neq 0$), yielding $\delta g \sim g^3$ and $\beta(g) = y_g g - B_4 g^3$. Interaction topology fixes the nonlinear term in $\beta(g)$ and defines distinct RG universality classes.

Here y_g sets the linear tendency of g under ω -coarse graining, while B_N sets the leading nonlinear saturation strength. Figure 4 then encodes the key distinction: CW self-renormalizes at order g^2 through the triadic channel, whereas GW self-renormalizes at order g^3 through the first available effective tetradic channel, enabled by a fi-

nite resonance width (detuning insertion $\Delta \neq 0$). Experimentally, the RG trajectory is traversed by tuning Re , which controls the strength of viscous dissipation relative to forcing at fixed driving frequency and injection geometry. Increasing Re weakens the viscous perturbation and allows $g(\omega)$ to grow smoothly from the near-Gaussian regime toward the topology-selected KZ fixed point. This topology-controlled saturation governs the renormalization of the global cascade response in discrete surface wave turbulence (DSWT), yielding the distinct power laws $\bar{\Sigma}_\omega(Re)$ in Fig. 3. Along the same flow, the inertial interval extends further into the ultraviolet before being arrested by viscosity, so the exit scale ω_K , and hence renormalized $\bar{\Omega}_\nu(Re^{1/2})$, increases with forcing as captured by the WF/Wegner scaling in Fig. 2. The attraction basin is therefore selected kinematically by dispersion (which fixes the resonant topology), while dissipation, tuned by Re , sets the crossover by controlling how far the flow proceeds along the corresponding RG trajectory toward its fixed point.

Relation to kinetic and discrete wave-turbulence theories.— Classical wave-turbulence (WT) theory is formulated in terms of kinetic equations that describe stationary Kolmogorov–Zakharov (KZ) fixed points and their inertial spectra [12, 13]. Discrete WT complements this by classifying integrable interaction graphs [18, 19]. In kinetic WT, interaction topology enters through the first non-vanishing collision integral [21]: I_3 for triads (CW) and I_4 for quartets (GW), while discrete WT identifies the corresponding resonant clusters [18].

The present Wilson–Fisher (WF) framework operates at a different level (Fig. 4): it does not replace kinetic or cluster theories, but organizes their inviscid fixed points into RG attraction basins using experimentally accessible coordinates $[\bar{\Omega}_\nu(N, y_g), \bar{\Sigma}_\omega(N, B_N)]$. These are orthogonal RG observables: $\bar{\Omega}_\nu$ measures the extent of the inertial basin (UV reach), while $\bar{\Sigma}_\omega$ measures its depth (response strength). Both are governed by the same interaction topology N , but probe distinct pieces of the RG physics: $\bar{\Omega}_\nu(N, y_g)$ is controlled by relevance and the viscous exit (linear RG/cutoff physics; Fig. 2 probes where the RG flow stops), whereas $\bar{\Sigma}_\omega(N, B_N)$ is controlled by nonlinear saturation and response (Wegner scaling; Fig. 3 probes how the RG flow proceeds).

Looking forward, DSWT offers a controlled route from discrete to statistical turbulence: increasing resonance broadening relative to mode spacing (or broadening the forcing band / enlarging the system) makes resonant clusters overlap and the effective interaction topology becomes statistical. In that limit, the present topology-controlled WF flows are expected to cross over toward the functional renormalization associated with fully developed Navier–Stokes turbulence [8, 11], positioning DSWT as an experimental bridge between discrete and continuous nonequilibrium criticality.